ORIGINAL PAPER

Check for updates

Rheological, morphological and solid-state viscoelastic properties of ethylene vinyl acetate copolymer/olefin block copolymer (EVA/OBC) blends

Nevra Ercan[1] · **Eylem Korkmaz[1]**

Abstract

In this study, the miscibility of ethylene vinyl acetate/olefin block copolymer (EVA/OBC) blends was investigated through the determination of melt-state viscoelastic properties as well as by morphological analysis using experimental and theoretical approaches. The SEM micrographs showed droplet-matrix morphology, and the blend containing a higher content of OBC exhibited the highest OBC-dispersed phase domain size. The complex viscosity of EVA/OBC blends showed a positive deviation from the log-additivity rule at all compositions, which indicates the strong interaction between phases. Cole–Cole and Han plots indicated miscibility in the molten state between EVA and OBC. The interfacial tension of EVA/OBC blends was determined by the implementation of Palierne and Bousmina emulsion models. Moreover, the blend samples were characterized in terms of creep properties using a dynamic mechanical analyzer, which demonstrated that the OBC increased the creep strains of the blends. The four-element Burger model and the Findley power law model were employed to model the creep behaviors of the EVA, OBC, and blend samples. The model predictions indicated that the incorporation of OBC into the EVA improved the creep rate of EVA/OBC blends significantly.

✉ Nevra Ercan
nevra.ercan@iuc.edu.tr

1 Department of Chemical Engineering, Faculty of Engineering, Istanbul University-Cerrahpasa, 34320 Avcılar, Istanbul, Turkey

Introduction

Polymer blending is a convenient technique for improving mechanical properties including impact resistance, abrasion resistance, and fracture behavior, as well as other properties such as easy printability and dimensional stability of polymeric materials. Polymer blends have a wide range of applications, and their properties are impacted by a variety of factors including the properties of individual components, the interfacial tension between components, and the morphology of the final material. The viscoelasticity, morphology, and processing properties of polymer blends are closely related to the rheological properties, which are of fundamental importance for industrial applications and also scientific studies.

In recent years, for the toughening of thermoplastics, scientific interest was tended toward blends containing thermoplastic elastomers (TPEs) than conventional vulcanized elastomer-based ones due to the easy processability and recyclability. Thermoplastic polyurethane, styrene block copolymers, polyolefinic TPEs, thermoplastic poly (ester–ether) elastomers and thermoplastic polyether-block-polyamide elastomers are commercially available polymers. TPEs can be used in the production of shoe soles, hoses, tubes, belts, housewares, sealing rings, and coatings. The olefin block copolymers (OBCs) are relatively new type of thermoplastic elastomers, and they were developed by Dow Chemical Co. via the chain shuttling polymerization [1]. OBC consists of crystallizable ethylene/octene blocks with very low octene content alternating with amorphous ethylene/octene blocks with high octene content [2]. OBCs have low density, higher crystallization and melting temperature, better elastic recovery, compression set, and abrasion resistance than almost same-density random copolymers having the same kind of olefin comonomer [2, 3]. These superior properties lead to many potential applications in the areas of elastic films, soft injection-molded articles, and profiles. Also, OBCs are used as an effective toughening agent for isotactic polypropylene, polypropylene random copolymer, polyamide 6, poly(lactic acid), and polyethylene [4–9]. According to the reported studies, OBC is an effective impact modifier for polyethylene, polypropylene homopolymer, and polypropylene random copolymer [4, 6, 7]. OBC is shown good compatibility with polyolefins due to the similar chain architecture. Furthermore, with the object of preparing shape memory materials and improving the viscoelastic properties of polymers, OBC was blended with polycaprolactone, polycaprolactone-poly(propylene carbonate), thermoplastic polyurethane–polycaprolactone, ethylene vinyl acetate, methyl vinyl silicone rubber and silicone rubber [10–16]. It was declared that OBC-based blends show an outstanding shape memory performance with high values of shape fixing and recovery.

EVA copolymers are random linear copolymers produced by copolymerization of ethylene and vinyl acetate. Commercial applications of EVAs vary depending on the vinyl acetate (VA) content of the copolymers. EVAs have been blended with different elastomers to improve their poor mechanical properties such as creep, tear, and abrasion resistance. In this study, OBC, a thermoplastic elastomer with a similar molecular structure, was selected for blending to improve

the performance of EVA products to be subjected to stress. To the best of our knowledge, no data on the solid-state viscoelastic properties of EVA (consisting of 18% vinyl acetate) and OBC blends have been published so far. Rheological experiments were employed to understand the compositional dependence of the miscibility of polymer blends. Additionally, scanning electron microscopy (SEM) observation was used to elucidate the phase morphology of EVA/OBC blends.

Experimental

Materials

EVA (Primeva® 1820F; vinyl acetate content = 18 wt%, density = 0.937 g/cm3, MFI at 190 °C and 2.16 kg = 2.0 g/10 min) was provided from REPSOLYPF Company, while OBC (Infuse™ 9077; density = 0.869 g/cm3, MFI at 190 °C and 2.16 kg = 0.5 g/10 min) was supplied by Dow Chemical Company. The weight percent of hard block and soft block was calculated 16 wt% and 84 wt%, respectively [2, 17].

Blend preparation

All polymers were dried in a vacuum oven overnight at 50 °C before melt processing. Polymers were manually premixed, and the mixture was melt blended in an internal mixer (RTX-M40 melt mixer, Kokbir, Turkey) at a temperature of 150 °C with a screw speed of 50 rpm for 10 min. The compositions of the samples are listed in Table 1.

Characterization

Morphological features of blend films were characterized by a field-emission scanning electron microscope (FE-SEM, FEI Quanta FEG 450) operated at 10 kV. Samples were cryo-fractured in liquid nitrogen and metallized with a thin gold layer. The particle size of the dispersed phase was measured by ImageJ 1.44p software. The number (D_n), mass (D_w) and volume (D_v) average of droplet

Table 1 Compositions of the samples

Sample	EVA (wt%)	OBC (wt%)
OBC	–	100
EVA	100	–
B10	90	10
B20	80	20
B30	70	30
B40	60	40
B50	50	50

diameter, the particle polydispersity (PD), and distance between particles (ID) of the dispersed OBC phase in the EVA matrix are calculated by Eqs. (1)–(5), respectively [18]:

$$D_{\mathrm{n}} = \frac{\sum n_i D_i}{\sum n_i} \tag{1}$$

$$D_w = \frac{\sum n_i D_i^2}{\sum n_i D_i} \tag{2}$$

$$D_{\mathrm{v}} = \frac{\sum n_i D_i^4}{\sum n_i D_i^3} \tag{3}$$

$$\mathrm{PD} = \frac{D_{\mathrm{v}}}{D_{\mathrm{n}}} \tag{4}$$

$$\mathrm{ID} = D_w \left[\left(\frac{\pi}{6 * \varphi} \right)^{\frac{1}{3}} - 1 \right] \tag{5}$$

where n_i is the number of the dispersed domains with diameter D_i measured from SEM images of at least 150 droplets, φ is the volumetric fraction of the dispersed phase.

Rheological behaviors of polymers and blend samples were characterized by performing different test procedures in the melt state in a rotational rheometer, AR-G2 (TA Instruments). Steady-state shear flow behaviors were measured in the shear rate range of 0.1–100 s^{-1} at 150 °C. Linear viscoelastic (LVE) regions of samples were determined by strain sweep tests, which were performed from an initial strain value of 0.1% to a final strain value of 100% with a frequency of 1 Hz at 150 °C. Then, frequency sweep tests were carried out in a frequency range of 0.1–100 Hz with a strain value (1%) in LVE region at 150 °C. Viscoelastic moduli (G' and G''), dynamic (or complex) viscosity ($\eta*$) values were recorded as a function of frequency. In each rheology test, a new sample was loaded to the rheometer and equilibrated to avoid possible effects of thermomechanical conditions and deformation history on the rheological response of the sample.

Solid-state viscoelastic properties of samples were measured with creep test conducted in a dynamic mechanical analyzer (DMA, SII Nanotechnology, ExStar 6100). Creep tests were performed by applying an instantaneous stress of 1 MPa at 25 °C for 15 min in uniaxial tensile test mode. Then applied stress was removed from the specimen, and creep recovery was followed for 15 min. Findley and Burger's models were fitted with Nonlinear Curve Fit analysis at OriginPro 8.1 software.

Results and discussion

Morphology

Figure 1a–d shows the micrographs of the B20 and B40 blend samples with different magnifications. The B20 blend displayed an apparent droplet-matrix morphology with a narrow distribution of OBC particle size corresponding to $D_n = 1.05$ µm, $D_w = 1.24$ µm, $D_v = 1.60$ µm and polydispersity of 1.5 (Fig. 1a and b). On the other hand, with the increase in the concentration of OBC, the droplets obviously were expanded due to the coalescence of dispersed phase in B40 sample. It seemed that the number average droplet (D_n) size changed from 1.05 to 1.17 µm, while the D_v changed from 1.6 to 2.6 µm, and the polydispersity (D_v/D_n) of OBC particles was 2.22. The interparticle distance of OBC in the EVA matrix decreased from 0.44 to 0.122 µm as the amount of OBC increased from 20 to 40 wt%. It can be seen from the figures that the morphologies changed from uniform droplets to partially continuous droplets with an increasing OBC content in the EVA matrix. However, no significant phase separation was observed in
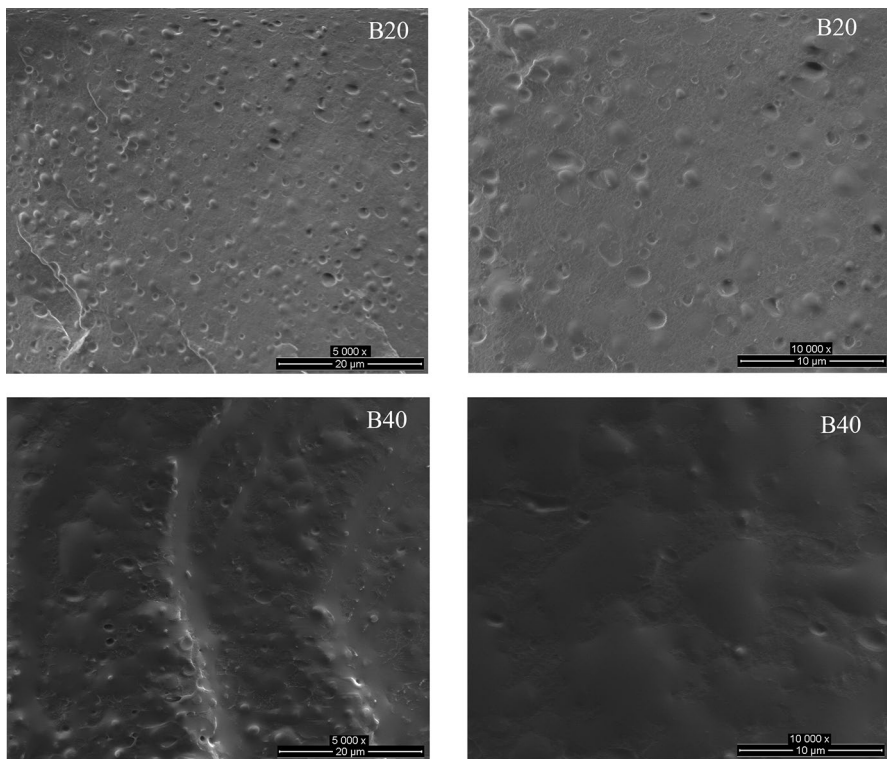

Fig. 1 SEM micrographs of EVA/OBC blends with different magnifications: **a** and **b** B20 blend, **c** and **d** B40 blend

both blend samples indicating sufficient compatibility and strong interaction between the EVA and OBC due to their olefinic structure.

Rheology

The rheological characterization can provide a link between the processing properties and structural characteristics of the blends. OBC and EVA are copolymers with different architectures. The block copolymers such as OBC have relatively narrow molecular weight distribution compared to EVAs, which have relatively broader molecular weight distribution due to the random structure [1, 2, 19, 20]. The morphology and the other physical properties of blends are related to the melt viscosities of each component.

Figure 2 depicts the flow curve of OBC, EVA and EVA/OBC blends as a function of shear rate at 150 °C. OBC showed Newtonian plateau at low shear rates (shear rates lower than 1 s^{-1}) and a shear thinning behavior at high shear rates. EVA and all blend compositions have a narrower transition Newtonian to non-Newtonian region and exhibited shear thinning behavior at lower shear rates than OBC. The shear viscosity of the EVA/OBC blends increased with the increase in the OBC copolymer content, but the increase in the amount of OBC did not affect the extent of the Newtonian region of the blends. In addition, the flow properties of samples were modeled by the Williamson [21] model to a high degree of accuracy, as displayed in Fig. 2, and the model parameters are listed in Table 2. Williamson model is defined as:

$$\eta = \frac{\eta_0}{1 + (K\dot{\gamma})^m} \tag{6}$$

where η_0 is the zero shear rate viscosity (Pa s), $\dot{\gamma}$ is the shear rate (s^{-1}), K is the consistency, and m is the shear-thinning index, where $m < 1$ indicates the shear-thinning behavior of polymers.
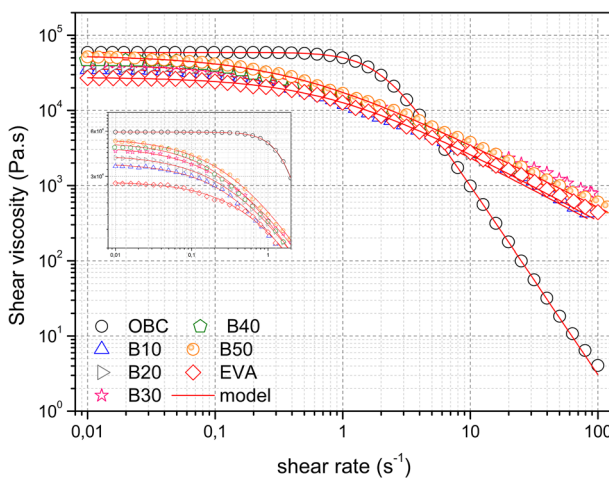

Fig. 2 Steady shear viscosity as a function of shear rate for EVA, OBC and EVA/OBC blends

Table 2 Williamson model parameters of samples

Sample	η_0 (Pa s)	K (s)	m	R^2
OBC	59,172	0.505	0.981	1
EVA	27,638	1.201	0.920	0.9992
B10	36,698	1.970	0.903	0.9999
B20	41,761	2.160	0.842	0.9996
B30	47,476	2.354	0.810	0.9994
B40	50,757	2.642	0.880	0.9968
B50	53,836	2.760	0.847	0.9995

OBC has relatively higher zero shear rate viscosity and higher critical shear rate (~2 s^{-1}) than EVA copolymer. EVA exhibited shear-thinning flow behavior at relatively small shear rates, which indicated that EVA possessed relatively broader molecular weight distribution than OBC, as reported in previous results [1, 2, 19, 20]. The zero shear viscosity of blends increased gradually with OBC content into EVA matrix due to the higher viscosity of OBC, and the transition from Newtonian plateau to shear-thinning regime was shifted to lower frequencies for blend samples. The critical shear rate is defined as the point at which the break-up limit curve crosses the coalescence one [22]. As the amount of OBC content increased in the blend composition, the critical shear rate decreased with increasing coalescence of OBC droplets. The critical shear rates of blends decreased gradually (EVA; 0.83 s^{-1}, B10; 0.51 s^{-1}, B20; 0.46 s^{-1}, B30; 0.42 s^{-1} B40; 0.38 s^{-1}, B50; 0.36 s^{-1}). This phenomenon can also be explained by Utracki's studies that, during blending, the viscosity of the system increased due to the formation of the entanglement of the minor phase in the major phase, and disentanglement and slippage existed at the interface that led to a deviation from the Newtonian region by increasing the shear rate [23–25].

Figure 3 illustrates the storage modulus (G') and the loss modulus (G'') of OBC, EVA, and EVA/OBC blends. The elastic and loss modulus of the blends laid between the OBC and EVA. At all frequency ranges, there was an increase in the G' of the EVA/OBC blends with the increase of OBC content.

In phase-separated polymer blends, the dispersed droplet phase leads to a shoulder in the frequency curve versus storage modulus at the low-frequency range. Shoulder formation in the curve is due to the shape relaxation of the dispersed phase droplets driven by the interfacial tension [26, 27]. The presence of the shoulder in the low-frequency region has been reported in polystyrene/poly(vinyl methyl ether), poly(styrene-co-acrylonitrile)/poly(methylmethacrylate), and polypropylene/ethylene-propylene-diene terpolymer blends due to the occurrence of phase separation [27–29]. Figure 3b shows a trend of loss modulus that is similar to the storage modulus counterpart. Furthermore, it was observed that loss modulus values of OBC and EVA were higher than their storage modulus, indicating that viscous behavior was more pronounced than the elastic behavior at low frequencies. As the frequency increases ($\omega_c > 10$ rad/s), the storage modulus appeared to be higher than the loss modulus due to the elastomeric nature of both copolymers.
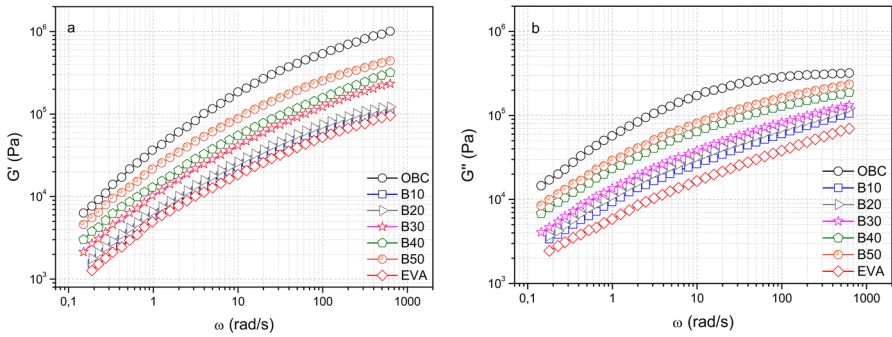
Fig. 3 a Storage modulus (G') and **b** loss modulus (G'') versus angular frequency of OBC, EVA and EVA/OBC blends at 150 °C

Figure 4 illustrates the variation of complex viscosity (η^*) as a function of angular frequency (ω) for the samples. Additionally, complex viscosity as a function of the OBC content obtained through the experimental data and the calculated data employing the logarithmic additivity rule at an angular frequency of $0.1\ s^{-1}$ is presented in Fig. 4. The log-additivity rule is expressed as [23]:

$$\log \eta^*(\omega) = \phi_1 \log (\eta^*(\omega))_1 + \left(1 - \phi_1\right) \log (\eta^*(\omega))_2 \tag{7}$$

It was clearly seen that the complex viscosity of the blend samples was slightly higher than that of EVA throughout the entire experimental frequency range. It could clearly be seen that EVA/OBC blends displayed a positive deviation
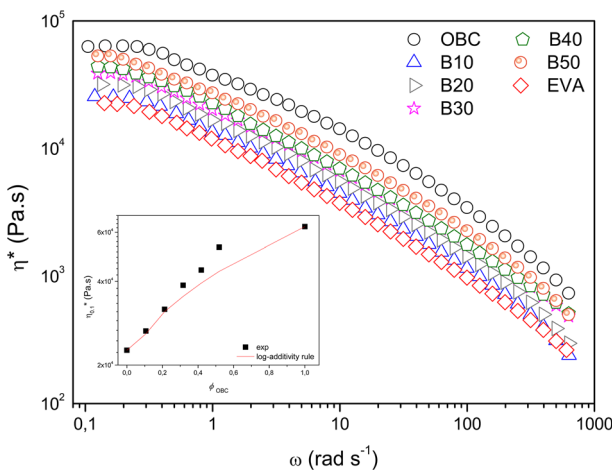

Fig. 4 Complex viscosity of OBC, EVA and EVA/OBC blends and calculated $\left(\eta_{0.1}^*\right)$ using log-additivity rule at angular frequency of $0.1\ s^{-1}$

behavior (PDB) in all compositions. PDB could be observed due to the presence of strong interfacial interaction between phases in blends [18, 23, 30, 31].

The melt compatibility of the polymer blends can be evaluated with the Han plots [32]. Han plots show a linear correlation in the plot of log G' versus log G''. The previous studies have shown that Han plot was independent of the temperature, and the slope of Han plot in the terminal zone was 2 for homopolymers and miscible blends in the molten state [32–35]. On the other hand, heterogeneous polymeric systems, such as mesophase and block copolymers, have slopes of less than 2. Lamnawar et al. used a Han plot to explore the miscibility of LLDPE/COC (cyclic olefin copolymer) blends [36]. They reported that the slope of Han plots had close values in pure polymers and blends, indicating the miscibility/compatibility of the blends of LLDPE/COC. The Han diagrams of OBC, EVA, and the blends with various compositions are presented in Fig. 5a.

The slope values of terminal zone were 1.27, 1.30, 1.26, 1.27, 1.27, 1.27, and 1.38 for OBC, B10, B20, B30, B40, B50, and EVA, respectively. The close slope values of the samples reflect the phase compatibility in the molten state [35–37].

Another method for interpreting the morphology of the blends is Cole–Cole plots, which consist of $\eta''\left(G'/\omega\right)$ versus $\eta'\left(G''/\omega\right)$. In Cole–Cole plots, it is assumed that miscible polymer blends show a single arc, while in multiphase blends a tail or even two circular arcs are observed [36, 38, 39]. From the findings, the EVA/OBC blends as well as OBC and EVA only present one circular arc on their Cole–Cole plots, indicating the miscibility of EVA and OBC phases in the melt state and the results consistent with the Han plots (Fig. 5b). In addition, as seen from the diagram, the radii of the arcs have increased with the increase of the OBC loading due to the high degree of entanglement of OBC [40, 41].

Several models, namely Palierne [42], Gramespacher and Meissner [43], Lee and Park [44] and Bousmina models [45], have been proposed to correlate the morphology and rheological properties of polymer blends. In this study, Palierne and Bousmina models were employed to predict the linear viscoelastic behavior of polymer blends and calculate the interfacial tension between EVA and OBC. Palierne and Bousmina emulsion models provide a constitutive equation for the complex modulus of a blend, viscoelastic property of both polymers, as a function of volume
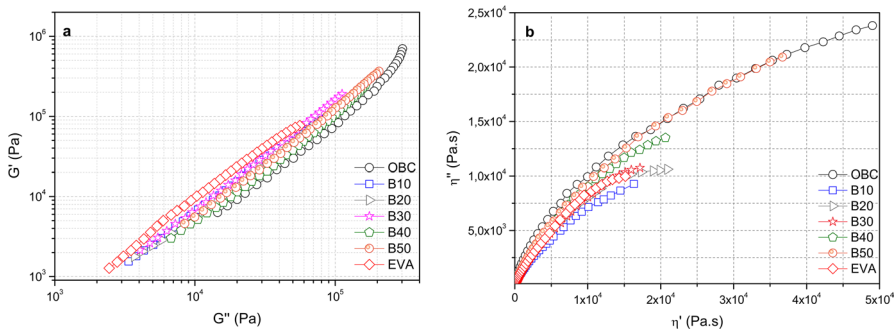

Fig. 5 **a** Han and **b** Cole–Cole plots of the samples

fraction of minor phase, volume average radius of dispersed phase and interfacial tension [42, 45]. The simplified Palierne model is expressed as:

$$G_b^*(\omega) = G_m^*(\omega)\frac{1 + 3\phi_d H(\omega)}{1 - 2\phi_d H(\omega)} \tag{8}$$

where

$$H(\omega) = \frac{4\left(\frac{\alpha}{R}\right)\left[2G_m^*(\omega) + 5G_d^*(\omega)\right] + \left[G_d^*(\omega) - G_m^*(\omega)\right]\left[16G_m^*(\omega) + 19G_d^*(\omega)\right]}{40\left(\frac{\alpha}{R}\right)\left[G_m^*(\omega) + G_d^*(\omega)\right] + \left[2G_d^*(\omega) + 3G_m^*(\omega)\right]\left[16G_m^*(\omega) + 19G_d^*(\omega)\right]} \tag{9}$$

The simplified Palierne's model can be used assuming a narrow size distribution ($D_v/D_n < 2.3$).

Bousmina's model in the following equation for the complex modulus of blend:

$$G_b^*(\omega) = G_m^*(\omega)\frac{2\left[G_d^*(\omega) + \left(\frac{\alpha}{R}\right)\right] + 3G_m^*(\omega) + 3\phi_d\left[G_d^*(\omega) + \left(\frac{\alpha}{R}\right) - G_m^*(\omega)\right]}{2\left[G_d^*(\omega) + \left(\frac{\alpha}{R}\right)\right] + 3G_m^*(\omega) - 2\phi_d\left[G_d^*(\omega) + \left(\frac{\alpha}{R}\right) - G_m^*(\omega)\right]} \tag{10}$$

where G_d^*, G_m^* and G_b^* are disperse, matrix and blend complex shear modulus, respectively. Parameter α is the interfacial tension between the components of the blend, ϕ_d is the volume fraction of dispersed phase and R is the radius of the dispersed phase.

The storage modulus (G') data for the blends of B20 and B40 were fitted using Palierne and Bousmina models, and the fitting curves were illustrated by red lines in Fig. 6a and b, respectively. It was clearly seen that the prediction accuracies of both models for B20 blend were higher than those of B40 blend. The deviation of the Palierne and Bousmina model values from the experimental data at high dispersed phase content were reported in COC/EVA, PMMA/PS, and PP/LDPE blends [31, 46–48]. The deviation of B40 blend could be attributed to the higher polydispersity (PD = 2.22) of the dispersed phase [46].
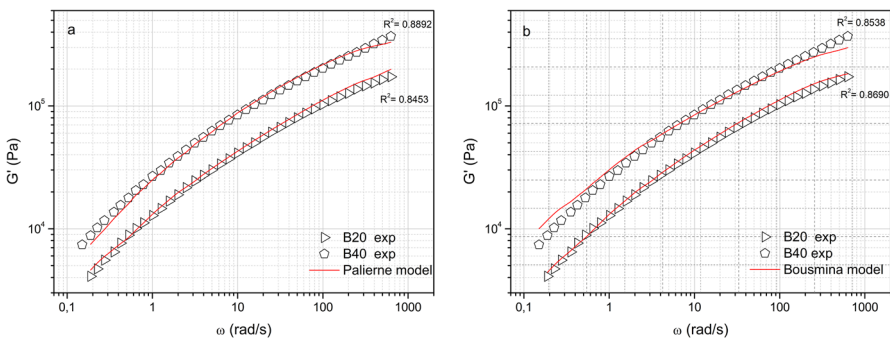

Fig. 6 **a** Palierne model and **b** Bousmina model estimations of (G′) for B20 and B40 blends

Based on the Palierne model, the calculated interfacial tensions for B20 and B40 blends were 0.0372 mN/m and 0.718 mN/m, respectively. By using the Bousmina model, the α values were found to be 0.0198 mN/m and 1.134 mN/m, respectively, for blends containing 20 and 40 wt% of OBC. These low interfacial tension values in EVA/OBC blends could be attributed to the existence of ethylene units in EVA and OBC and as a result a strong intermolecular interaction in EVA/OBC blends.

Creep and recovery of blends

Creep–recovery test is an analytical method to understand the material behavior and evaluates the service life of a product. Figure 7a and b depicts the experimental creep and creep-recovery strain curves as a function of time for OBC (Fig. 7a) and EVA/OBC blend samples (Fig. 7b) when a constant stress of 1 MPa was applied. It was clear from the plot (Fig. 7a) that an instantaneous deformation with relatively high strain rate occurs as a consequence of application of the constant stress due to the elastomeric nature of OBC. OBC displayed high instantaneous creep strain (approx. 160% at the end of 15 min.) and considerable elastic recovery (91%) where EVA showed only 4% of the initial creep strain. Compared to the previous results, it can be said that the VA content of EVA was inversely proportional to the creep resistance [15]. The recovered strain of EVA with 18 wt% of VA (86%) was lower than EVA with 12 wt% VA (92%) and higher than EVA with 28 wt% VA (84%) at the end of recovery time (15 min). In all blend samples, the creep strain values were increased continually with the increase of OBC content in compositions due to the elastomeric characteristics of OBC. In comparison with EVA, the creep strains of EVA/OBC blends increased by 11%, 51%, 66%, 89% and 168%, respectively. In the recovery region, the elastic deformation of all blends disappears instantly, and the elastic recovery of the samples (86–88%) was found approximately the same as EVA.

In order to better understand the influence of OBC on the creep and recovery behaviors of EVA blends, two viscoelastic constitutive models, Burger's and Findley's power law were applied. Burger's four-element model is a series combination of the Maxwell and Kelvin–Voigt models. The total creep strain is divided into three
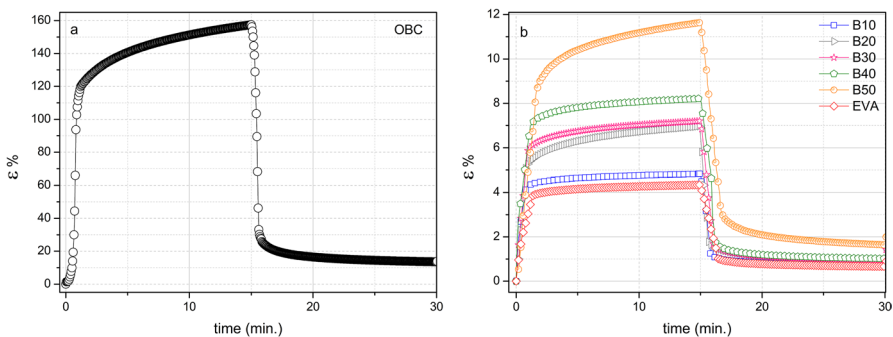

Fig. 7 Experimental creep and recovery behavior of **a** OBC, **b** EVA and EVA/OBC blend samples

separate parts: the instantaneous elastic deformation (Maxwell spring, ε_M), viscoelastic deformation (Kelvin unit, ε_K), and viscous deformation (Maxwell dash-pot, ε_∞). The total strain as a function of time ε is given by the following equations:

$$\varepsilon(t) = \varepsilon_M + \varepsilon_K + \varepsilon_\infty \tag{11}$$

$$\varepsilon(t) = \frac{\sigma}{E_M} + \frac{\sigma}{E_K}\left[1 - exp\left(-\frac{E_K t}{\eta_K}\right)\right] + \frac{\sigma t}{\eta_M} \tag{12}$$

where $\varepsilon(t)$ is the creep strain, σ is the applied stress, t is the time, E_M and E_K are the elastic moduli of Maxwell and Kelvin springs, respectively, η_M and η_K are the viscosities of Maxwell and Kelvin dashpots, respectively [49, 50]. Retardation time (τ_0) is for the Kelvin element to produce 63.21% of its total deformation and creep rate ($\dot{\varepsilon}$) can be found using the following equations:

$$\tau_0 = \frac{\eta_K}{E_K} \tag{13}$$

$$\dot{\varepsilon} = \frac{\sigma}{\eta_M} \tag{14}$$

Another analytical model, Findley's power law model was also applied to understand structure–property relationship of the blends.

$$\varepsilon(t) = \varepsilon_0 + At^n \tag{15}$$

where $\varepsilon(t)$ is the creep strain, t is the time, ε_0 is the time-independent strain, A is the amplitude of transient creep strain, a time-dependent term; and n is stress-independent time exponent, with values usually less than 1 [51].

The experimental data and model fittings are presented in Fig. 8, and the parameters for both models are given in Table 3. The implementation of both models provides good fits to the experimental data. The modulus of Maxwell spring (E_M) represents instantaneous creep strain, which could be immediately recovered on the removal of stress. As seen in Table 3, OBC exhibited typical elastomeric behavior with low modulus values corresponding to high creep strains with very low irrecoverable creep (η_M). The time-dependent E_K and η_K in the Kelvin unit can be associated with the stiffness and viscous or orientated flow of amorphous polymer chains in short term, respectively [50]. The data indicate that OBC chains promptly oriented in a short-term period once the stress loaded. EVA displayed relatively higher elastic modulus values (E_M, E_K) than OBC. For blends, the values of modulus and irrecoverable creep strain decreased with an increasing OBC content, these results indicated that decrease in the stiffness in blends and also an improvement in the elastic recovery of blends. The creep rate is a characteristic parameter that determines the dimensional stability of materials. In all blend compositions, these values tend to increase with the addition of OBC due to higher elasticity compared to EVA.

The fitted results of Findley's power law model of creep curves are also summarized in Table 3. The time-independent strain ε_0 and time-dependent term A showed
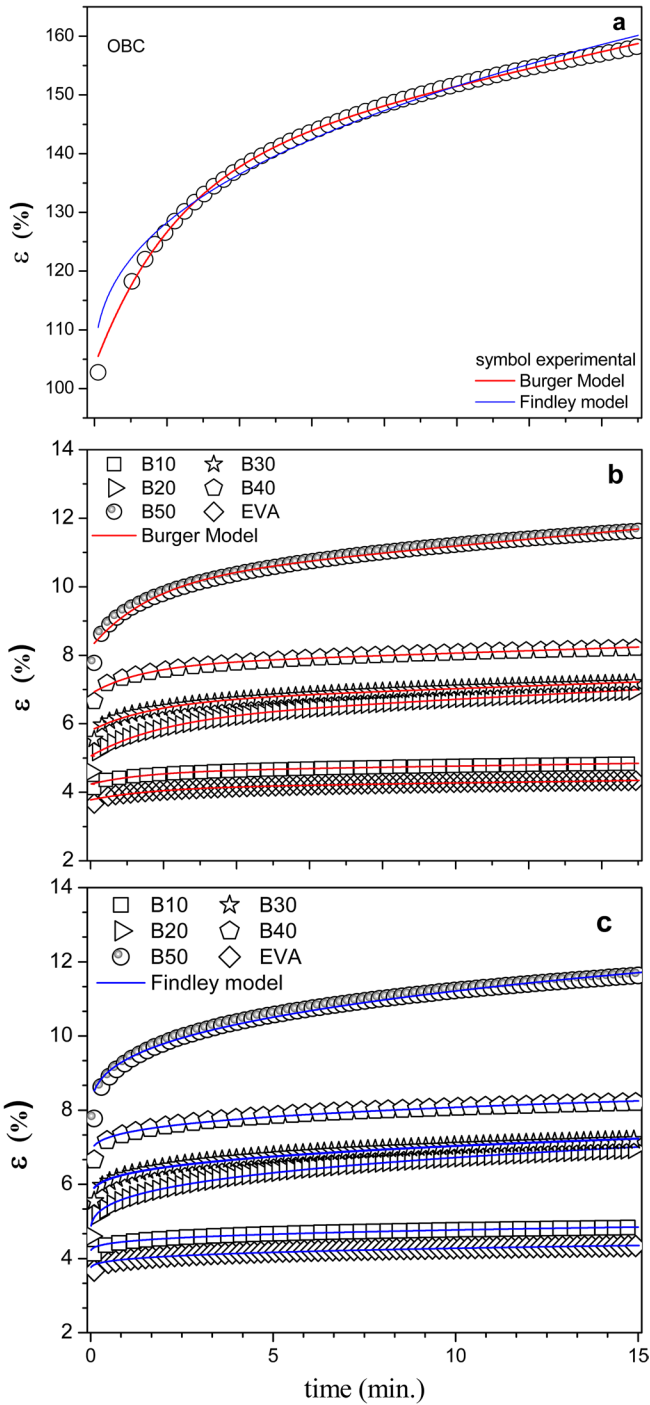
Fig. 8 Creep curves of samples **a** OBC, **b** and **c** EVA and EVA/OBC blends (symbols represent experimental data and lines represent the model fits)

Table 3 Burger and Findley model parameters of the samples

Sample	Burger parameters							Findley parameters			
	E_M (MPa)	E_K (MPa)	η_M (GPa s)	η_K (GPa s)	τ_0 (s)	$\dot{\varepsilon}(10^{-6})$ (s^{-1})	R^2	ε_0 (%)	A (10^{-2})	n	R^2
OBC	0.96	2.92	4.4	0.4	137	230	0.9992	102.7	19.3	0.40	0.9828
EVA	26.5	283.8	418	29.5	104	2.4	0.9949	3.7	0.31	0.29	0.9897
B10	23.9	275.3	370	25.2	92	2.7	0.9917	4.2	0.34	0.29	0.9934
B20	19.8	119.1	155	12.2	102	6.5	0.9947	4.6	0.48	0.31	0.9972
B30	17.2	98.9	109	10.9	110	9.2	0.9943	5.5	0.73	0.31	0.9883
B40	14.6	89.9	92	10.1	112	10.9	0.9796	6.7	0.75	0.31	0.9899
B50	12.2	42.6	61	5.1	120	16.4	0.9948	7.8	1.61	0.33	0.9886

significant increments with the incorporation of the elastomeric phase. The exponent "n" increased with the increasing OBC content, which suggests that the blends would spend less time to achieve a certain creep level with the applied stress.

Conclusions

In this study, the effect of OBC content on the morphological and solid-state creep properties as well as the rheological behavior of EVA/OBC blends was investigated. Morphology studies of blends revealed that OBC dispersed throughout the EVA continuous matrix as droplets and the domain size became larger with increasing content of OBC; however, no phase separation was observed. From the rheological measurements, it was observed that the complex viscosity of all blends illustrated positive deviation from the log-additivity rule, which pointed out the strong interaction between EVA and OBC. Cole–Cole plots and Han plots indicated the miscibility between EVA and OBC phases; these results corroborated the morphology analysis. The Bousmina and Palierne predictions were used to obtain the interfacial tension between EVA and OBC, which was found to be 0.0198–0.0372 mN/m for 80/20 EVA/OBC blends and 1.1344 and 0.718 mN/m for 60/40 EVA/OBC blends, respectively. The solid-state creep-recovery test showed that OBC affected the creep strains of the blends without altering elastic recovery.

Declarations

Conflict of interest The authors declare that they have no known competing financial interests or personal relationships that could have appeared to influence the work reported in this manuscript.

References

1. Arriola DJ, Carnahan EM, Hustad PD et al (2006) Catalytic production of olefin block copolymers via chain shuttling polymerization. Science 80(312):714–719. https://doi.org/10.1126/science.1125268
2. Wang HP, Khariwala DU, Cheung W et al (2007) Characterization of some new olefinic block copolymers. Macromolecules 40:2852–2862. https://doi.org/10.1021/ma061680e
3. Chum PS, Swogger KW (2008) Olefin polymer technologies-History and recent progress at the Dow chemical company. Prog Polym Sci 33:797–819. https://doi.org/10.1016/j.progpolymsci.2008.05.003
4. Dias P, Lin YJ, Poon B et al (2008) Adhesion of statistical and blocky ethylene-octene copolymers to polypropylene. Polymer 49:2937–2946. https://doi.org/10.1016/j.polymer.2008.04.022
5. Liu G, Zhang X, Li X et al (2012) Correlation of miscibility and mechanical properties of polypropylene/olefin block copolymers: effect of chain composition. J Appl Polym Sci 125:666–675. https://doi.org/10.1002/app.36244
6. Ren Q, Fan J, Zhang Q et al (2016) Toughened polypropylene random copolymer with olefin block copolymer. Mater Des 107:295–301. https://doi.org/10.1016/j.matdes.2016.06.052
7. Zhang Q, Fan J, Feng J, Lu X (2015) Regulation of crystalline morphologies and mechanical properties of olefin multiblock copolymers by blending polymer with similar architecture of constituent blocks. Polymer 73:139–148. https://doi.org/10.1016/j.polymer.2015.07.034

8. Wu M, Wu Z, Wang K et al (2014) Simultaneous the thermodynamics favorable compatibility and morphology to achieve excellent comprehensive mechanics in PLA/OBC blend. Polymer 55:6409–6417. https://doi.org/10.1016/j.polymer.2014.10.004

9. Lin X, Liu Y, Chen X et al (2020) Reactive compatibilization of polyamide 6/olefin block copolymer blends: phase morphology, rheological behavior, thermal behavior, and mechanical properties. Materials 13:1146. https://doi.org/10.3390/ma13051146

10. Lai SM, You PY, Chiu YT, Kuo CW (2017) Triple-shape memory properties of thermoplastic polyurethane/olefin block copolymer/polycaprolactone blends. J Polym Res. https://doi.org/10.1007/s10965-017-1319-z

11. Lai SM, Li CH, Kao HC, Liu LC (2019) Shape memory properties of melt-blended olefin block copolymer (OBC)/ethylene-vinyl acetate blends. J Macromol Sci Part B Phys 58:174–191. https://doi.org/10.1080/00222348.2018.1558593

12. Yang ZX, Chen Y, Liu X et al (2020) Fabrication of poly(ε-caprolactone) (PCL)/poly(propylene carbonate) (PPC)/ethylene-α-octene block copolymer (OBC) triple shape memory blends with cycling performance by constructing a co-continuous phase morphology. Polym Int 69:702–711. https://doi.org/10.1002/pi.6005

13. Lai SM, Fan Jiang SY, Chou HC et al (2021) Novel two-way multiple shape memory effects of olefin block copolymer (OBC)/polycaprolactone (PCL) blends. Polym Test 102:107333. https://doi.org/10.1016/j.polymertesting.2021.107333

14. Lai S-M, Chen Y-J, Yu BY (2021) Preparation and characterization of two-way shape memory olefin block copolymer/silicone elastomeric blends. J Appl Polym Sci 138:e51238. https://doi.org/10.1002/app.51238

15. Ercan N, Korkmaz E (2021) Structural, thermal, mechanical and viscoelastic properties of ethylene vinyl acetate (EVA)/olefin block copolymer (OBC) blends. Mater Today Commun 28:102634. https://doi.org/10.1016/j.mtcomm.2021.102634

16. Ren Q, Wang XJ, Zhao YQ et al (2021) Thermo-responsive shape memory behavior of methyl vinyl silicone rubber/olefin block copolymer blends via co-crosslinking. Int Polym Process 36:26–34. https://doi.org/10.1515/ipp-2020-3927

17. Zuo F, Burger C, Chen X et al (2010) An in situ x-ray structural study of olefin block and random copolymers under uniaxial deformation. Macromolecules 43:1922–1929. https://doi.org/10.1021/ma902105v

18. Faker M, Razavi Aghjeh MK, Ghaffari M, Seyyedi SA (2008) Rheology, morphology and mechanical properties of polyethylene/ethylene vinyl acetate copolymer (PE/EVA) blends. Eur Polym J 44:1834–1842. https://doi.org/10.1016/j.eurpolymj.2008.04.002

19. Park HE, Dealy JM, Marchand GR et al (2010) Rheology and structure of molten, olefin multiblock copolymers. Macromolecules 43:6789–6799. https://doi.org/10.1021/ma1012122

20. Arsac A, Carrot C, Guillet J (1999) Rheological characterization of ethylene vinyl acetate copolymers. J Appl Polym Sci 74:2625–2630. https://doi.org/10.1002/(SICI)1097-4628(19991209)74:11%3c2625::AID-APP9%3e3.0.CO;2-G

21. Williamson RV (1929) The flow of pseudoplastic materials. Ind Eng Chem 21:1108–1111. https://doi.org/10.1021/ie50239a035

22. Minale M, Moldenaers P, Mewis J (1997) Effect of shear history on the morphology of immiscible polymer blends. Macromolecules 30:5470–5475. https://doi.org/10.1021/ma9617330

23. Utracki LA, Kanial MR (1982) Melt rheology of polymer blends. Polym Eng Sci 22:96–114. https://doi.org/10.1002/pen.760220211

24. Utracki LA (1991) On the viscosity-concentration dependence of immiscible polymer blends. J Rheol 35:1615–1637. https://doi.org/10.1122/1.550248

25. Hajiraissi R (2020) Linear and nonlinear melt viscoelastic properties of fibrillated blend fiber based on polypropylene/polytrimethylene terephthalate. Polym Bull 77:2423–2442. https://doi.org/10.1007/s00289-019-02865-1

26. Khademzadeh Yeganeh J, Goharpey F, Foudazi R (2012) Can only rheology be used to determine the phase separation mechanism in dynamically asymmetric polymer blends (PS/PVME)? RSC Adv 2:8116–8127. https://doi.org/10.1039/c2ra21307a

27. Khademzadeh Yeganeh J, Goharpey F, Foudazi R (2010) Rheology and morphology of dynamically asymmetric LCST blends: polystyrene/poly(vinyl methyl ether). Macromolecules 43:8670–8685. https://doi.org/10.1021/ma101421s

28. Bousmina M, Lavoie A, Riedl B (2002) Phase segregation in SAN/PMMA blends probed by rheology, microscopy, and inverse gas chromatography techniques. Macromolecules 35:6274–6283. https://doi.org/10.1021/ma020053w

29. Zhang Z, Yu F, Zhou N, Zhang H (2015) Compatibilization by olefin block copolymer (OBC) in polypropylene/ethylene-propylene-diene terpolymer (PP/EPDM) blends. J Macromol Sci Part B Phys 54:159–176. https://doi.org/10.1080/00222348.2014.996497

30. Chen Y, Zou H, Liang M, Liu P (2013) Rheological, thermal, and morphological properties of low-density polyethylene/ultra-high-molecular-weight polyethylene and linear low-density polyethylene/ultra-high-molecular-weight polyethylene blends. J Appl Polym Sci 129:945–953. https://doi.org/10.1002/app.38374

31. Jafari SH, Hesabi MN, Khonakdar HA, Asl-Rahimi M (2011) Correlation of rheology and morphology and estimation of interfacial tension of immiscible COC/EVA blends. J Polym Res 18:821–831. https://doi.org/10.1007/s10965-010-9479-0

32. Dae Han C, Kim J (1987) Rheological technique for determining the order-disorder transition of block copolymers. J Polym Sci Part B Polym Phys 25:1741–1764. https://doi.org/10.1002/polb.1987.090250815

33. Walha F, Lamnawar K, Maazouz A et al (2016) Rheological, morphological and mechanical studies of sustainably sourced polymer blends based on poly(lactic acid) and polyamide 11. Polymers. https://doi.org/10.3390/polym8030061

34. Kwag H, Rana D, Cho K et al (2000) Binary blends of metallocene polyethylene with conventional polyolefins: rheological and morphological properties. Polym Eng Sci 40:1672–1681. https://doi.org/10.1002/pen.11299

35. Yoon KH, Park S, Kim YC (2012) Study of the rheological properties and crystallization behavior of branched PP/silicate composites. Polym J 44:1098–1104. https://doi.org/10.1038/pj.2012.68

36. Lamnawar K, Vion-Loisel F, Maazouz A (2010) Rheological, morphological, and heat seal properties of linear low density polyethylene and cyclo olefine copolymer (LLDPE/COC) blends. J Appl Polym Sci 116:2015–2022. https://doi.org/10.1002/app.31804

37. Khonakdar HA, Jafari SH, Hesabi MN (2015) Miscibility analysis, viscoelastic properties and morphology of cyclic olefin copolymer/polyolefin elastomer (COC/POE) blends. Compos Part B Eng 69:111–119. https://doi.org/10.1016/j.compositesb.2014.09.034

38. Cole KS, Cole RH (1941) Dispersion and absorption in dielectrics I. Alternating current characteristics. J Chem Phys 9:341. https://doi.org/10.1063/1.1750906

39. Codou A, Anstey A, Misra M, Mohanty AK (2018) Novel compatibilized nylon-based ternary blends with polypropylene and poly(lactic acid): morphology evolution and rheological behaviour †. RSC Adv 8:15709–15724. https://doi.org/10.1039/c8ra01707g

40. Huang Y, He Y, Ding W et al (2017) Improved viscoelastic, thermal, and mechanical properties of in situ microfibrillar polypropylene/ polyamide 6,6 composites via direct extrusion using a triple-screw extruder. RSC Adv 7:5030–5038. https://doi.org/10.1039/c6ra26734c

41. Tian J, Yu W, Zhou C (2006) The preparation and rheology characterization of long chain branching polypropylene. Polymer 47:7962–7969. https://doi.org/10.1016/j.polymer.2006.09.042

42. Palierne JE (1990) Linear rheology of viscoelastic emulsions with interfacial tension. Rheol Acta Rheol Acta 29:204–214. https://doi.org/10.1007/BF01331356

43. Gramespacher H, Meissner J (1992) Interfacial tension between polymer melts measured by shear oscillations of their blends. J Rheol 36:1127–1141. https://doi.org/10.1122/1.550304

44. Lee HM, Park OO (1994) Rheology and dynamics of immiscible polymer blends. J Rheol 38:1405–1425. https://doi.org/10.1122/1.550551

45. Bousmina M (1999) Rheology of polymer blends: linear model for viscoelastic emulsions. Rheol Acta 38:73–83. https://doi.org/10.1007/s003970050157

46. Calvão PS, Yee M, Demarquette NR (2005) Effect of composition on the linear viscoelastic behavior and morphology of PMMA/PS and PMMA/PP blends. Polymer 46:2610–2620. https://doi.org/10.1016/j.polymer.2005.02.010

47. Jozaghkar MR, Jahani Y, Arabi H, Ziaee F (2019) Effect of polyethylene molecular architecture on the dynamic viscoelastic behavior of polyethylene/polyhexene-1 blends and its correlation with morphology. Polym Technol Mater 58:560–572. https://doi.org/10.1080/03602559.2018.1493125

48. Liao H, Liao R, Li S et al (2021) Rheology of a polypropylene/low-density polyethylene blending melt: fitting dynamic rheological data by Palierne model and Lee and Park model. Polym Bull 79:4957–4970. https://doi.org/10.1007/s00289-021-03720-y

49. Findley WN, Lai JS, Onaran K (1976) Creep and relaxation of nonlinear viscoelastic materials: with an introduction to linear viscoelasticity. North Holland Publishing Company, New York
50. Yang JL, Zhang Z, Schlarb AK, Friedrich K (2006) On the characterization of tensile creep resistance of polyamide 66 nanocomposites. Part II: modeling and prediction of long-term performance. Polymer 47:6745–6758. https://doi.org/10.1016/j.polymer.2006.07.060
51. Xu Y, Wu Q, Lei Y, Yao F (2010) Creep behavior of bagasse fiber reinforced polymer composites. Bioresour Technol 101:3280–3286. https://doi.org/10.1016/j.biortech.2009.12.072